JOURNAL OF MATERIALS SCIENCE 24 (1989) 485–492

Formation, compressibility and sintering of aggregated MgO powder

LI NAN
Department of Materials Science and Engineering, Wuhan Iron and Steel University, Wuhan, China

The aggregates of MgO crystallites are formed during calcination. The compressibility of the aggregated MgO powder and the sintering of the compacts of the aggregated MgO powders, as well as the grain growth of MgO were investigated.

1. Introduction

Magnesia is obtained by decomposition of magnesite or magnesium hydrate. Usually the contour of particles of the originals remains after decomposition. One calls them "pseudomorph". In fact, pseudomorphs are MgO crystallite aggregates which hold the contour of the original particles. China is rich in magnesite. This paper is a review of the investigations on sintering of aggregated MgO powder obtained from magnesite [1–3].

2. Sintering of MgO crystallite in the aggregates during calcination

The chemical composition of magnesite used in this study is given in Table I. The particle size of magnesite is in the range from 44 to 75 μm.

The isothermal calcination of magnesite samples of about 0.8 g was carried out at 730, 880, 930 and 1030° C for 1.5, 3, 6, 10, 20, 50, 100 and 140 min, respectively.

A typical TEM micrograph of MgO powder sample is given in Fig. 1. It is an aggregate packed with MgO crystallites.

The surface area and distribution of pores of the powder were determined by the BET method. The dependence of the surface area on soaking time is shown in Fig. 2. It can be seen that in the first 20 min, the surface area decreases very fast with increasing soaking time, but the rate of decrease becomes less lowers with increasing soaking time. It was found that after calcination at 730° C for 1.5 min, the Ig-loss of magnesite powder reached 97% of the total amount of Ig-loss, so that the calcination after 1.5 min should be the sintering of the powders of MgO. The surface area reduction models can be used to analyse data obtained in our study.

Komatsu *et al.* [4] assumed that the neck growth and surface flattening took place concurrently by surface diffusion during sintering. The surface area change ΔS is equal to the sum of two surface area changes

$$\Delta S = \Delta S_1 + \Delta S_2 \quad (1)$$

where ΔS_1 is due to the neck growth and ΔS_2 to the surface flattening

$$\Delta S_1 = Gt^{2/7} \quad (2)$$

$$\Delta S_2 = Ht^{1/2} \quad (3)$$

where G and H are constants.

$$\frac{S}{t^{2/7}} = G + Ht^{3/14} \quad (4)$$

The data obtained in our study do not obey Equation 4 but obey Equation 5. (Fig. 3)

$$S = A + Gt^{2/7} \quad (5)$$

This demonstrates that the neck growth is the predominant factor and surface flattening is not important. The changes of the slope of the straight lines at about 20 min, ($t^{2/7} = 2.35$) might result from change of mechanism.

German [5] reported that for initial-stage sintering the surface area reduction kinetics can be expressed as

$$\left(\frac{\Delta S}{S_0}\right) r = kt \quad (6)$$

where r is the mechanism-dependent exponent, $\Delta S/S_0$ the loss in surface area ΔS divided by the initial surface area S_0, t the sintering time and k a constant.

The variations of $(\Delta S/S_0)$ with soaking time are shown in Fig. 4. This indicates that for calcination at 730° C, the data do not obey Equation 6, but for calcination at 880° C, the plot of log $(\Delta S/S_0)$ against log t shows two straight lines with different slopes. For line 1 (log $t < 1.24$), the exponent r is equal to about two; it is between 1.5 and 3.5 which were reported by German for evaporation–condensation and surface

TABLE I The chemical composition of magnesite (wt %)

MgO	CaO	Fe_2O_3	Al_2O_3	SiO_2	Ig-loss
47.24–47.64	0.24–0.29	0.47–0.62	0.08–0.45	0.26–0.72	51.00–51.11

0022–2461/89 $03.00 + .12

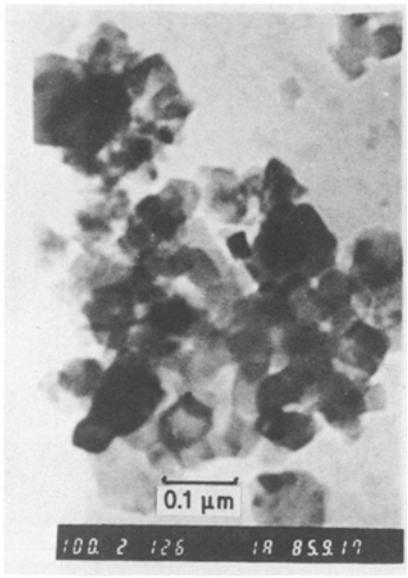

Figure 1 TEM micrograph of MgO aggregates calcined at 1030° C for 50 min.

diffusion, respectively. In addition, a limit established by German for the initial-stage sintering is $\Delta S/S_0 = 0.5$. In our study we have $\Delta S/S_0 = 0.58$ for line 1. However, line 2 ($\log t > 1.24$) also is a satisfactory straight line, even though $\Delta S/S_0 > 0.5$, r is equal to 8.7, much more than any value of the exponent r proposed by German.

The grain growth also shows some mechanism transformations during calcination (Fig. 5).

To seek the transformation of mechanism during calcination, the pore size distribution was determined by the BET method, as shown in Fig. 6, and the data are given in Table II. The pore diameters measured by BET method are smaller than 40 nm, so that we assume they are pores within the MgO aggregates.

It is found that calcination process at 880° C can be

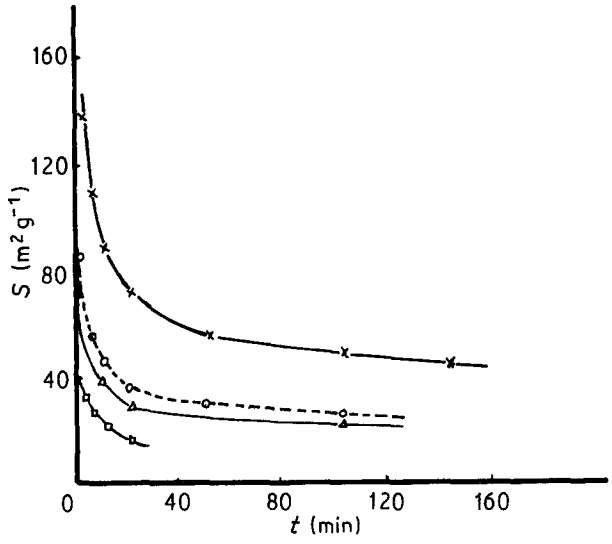

Figure 2 Dependence of the surface area of MgO powder on soaking time. (x calcined at 730° C, o calcined at 880° C, △ calcined at 930° C, □ calcined at 1030° C)

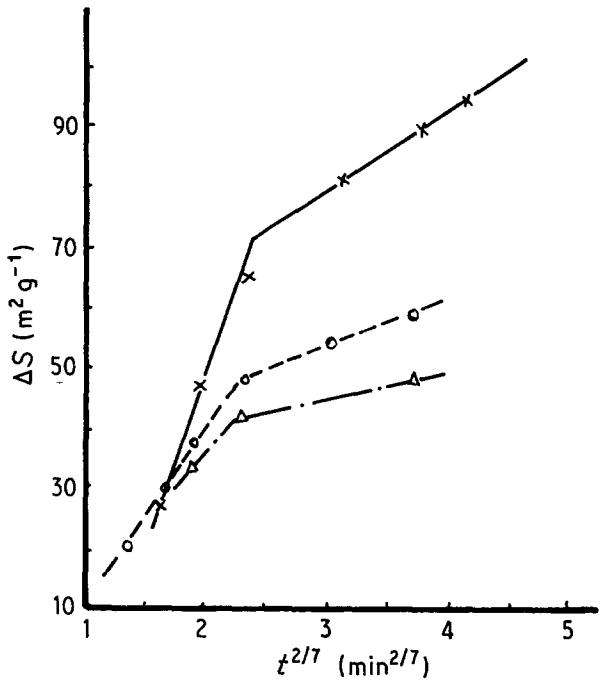

Figure 3 The dependence of ΔS on soaking time for samples calcined at 730° C (x) (t_0 = 3 min, S_0 = 139.8 m^2 g^{-1}) at 880° C (o) (t_0 = 1.5 min, S_0 = 85.8 m^2 g^{-1}) and at 930° C (t_0 = 1.5 min, S_0 = 73.1 m^2 g^{-1}).

divided in to three stages. In the period between 1.5 and 3.0 min, the specific volume of pores and the porosity decrease accompanied by an increment of median, mode and shrinkage for magnesite particle. In this short period, the adjustment of MgO crystallites may be the predominant mechanism. In the period from 3.0 to 20.0 min, the specific volume of pores, the shrinkage for magnesite and porosity of aggregates changes little, accompanied by an increment of median and mode, that means the small pores grow rapidly. The evaporation–condensation and surface diffusion mechanisms may take place concurrently in this stage; the evaporation–condensation mechanism should be more important as r in Equation 6 is equal to two. From 20 to 50 min, the specific volume of pore, median and porosity decrease accompanied by an increment of shrinkage for magnesite. The volume diffusion and/or grain boundary diffusion should be considered to have effects in this stage. Althugh the data obtained in our studies obey Equation 5, proposed by Komatsu *et al.* [4], the

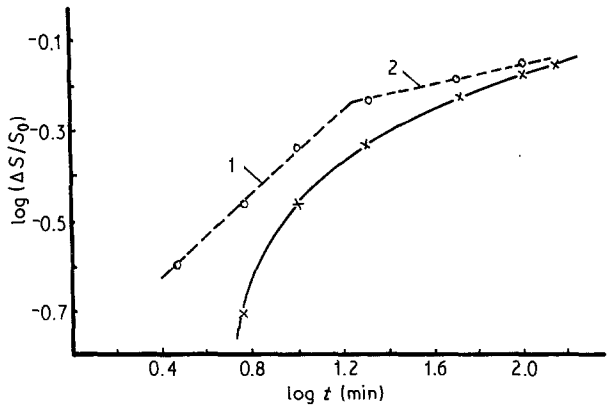

Figure 4 Variation of log ($\Delta S/S_0$) with log t (x 730° C, o 880° C).

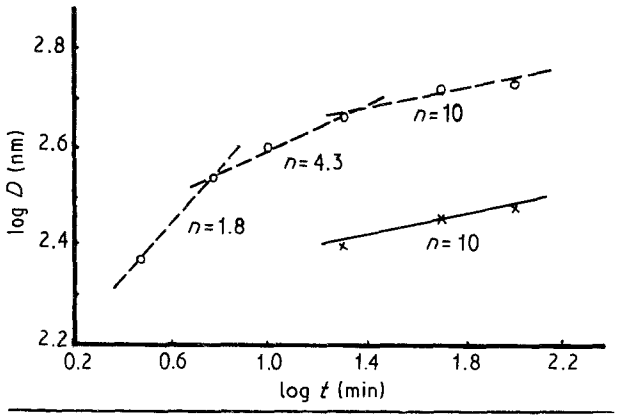

Figure 5 Grain size as a function of soaking time (× 730° C, ○ 880° C).

diffusion coefficients calculated from G in Equation 5 not only include the contribution of surface diffusion but also the contribution of other mechanisms. In addition, the surface diffusion coefficient, $D_s = 1.51 \times 10^{-8} \exp(-163/RT)$ (kJ mol^{-1}), which we reported in an earlier paper [6] should involve the contribution of other mechanisms.

3. Compression of aggregated MgO powder and sintering of compacts

The aggregated MgO powder was pressed without a binder. As the aggregates themselves are made up of MgO crystallites, and the aggregates pack together to form a compact, there are two classes of pores in the compacts: (1) pores inside the aggregates and between the crystallites, they are thought to be smaller than 40 nm, (2) pores between the aggregates. We call the former "first pore" and the latter "secondary pore". Van de Ben and Hunter [7], Sacks and Pask [8], and Lang [9] studied sintering of agglomerated powders, they proposed that three classes of pores exist in the compacts. However, in our study the aggregates of MgO crystallites were partially sintered and difficult to hold together by Van der Waals force to form agglomerates, so only two classes of pore are considered.

The specific volume of secondary pores was obtained by Equation 7, assuming that the aggregates do not break down.

$$C = \frac{1}{\gamma} - \left(\frac{1}{\varrho} + V_s\right) \qquad (7)$$

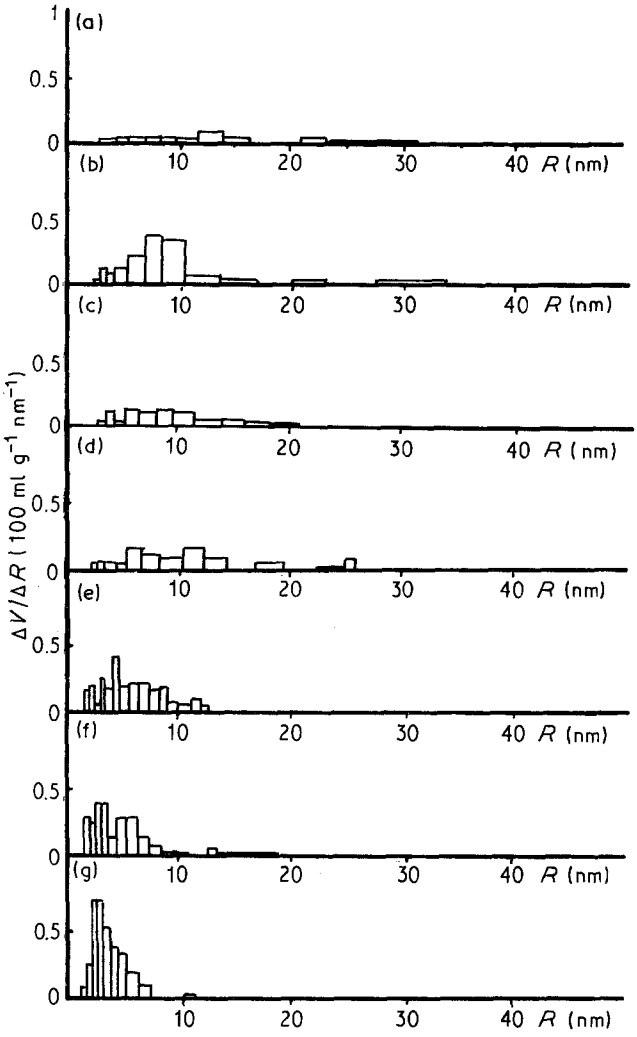

Figure 6 Distribution of pore size in the aggregates of MgO, calcined at (a) 1030° C for 50 min, (b) 730° C for 50 min, (c) 880° C for 50 min, (d) 880° C for 20 min, (e) 880° C for 6 min, (f) 880° C for 3 min and (g) 880° C for 1.5 min.

where C is the specific volume of secondary pores (cm^3 g^{-1}), γ the bulk density of green compacts (g cm^{-3}), ϱ the density of MgO, 3.58 (g cm^{-3}), V_s is the specific volume of first pores (cm^3 g^{-1}).

The dependence of bulk density of the compacts and specific volume of secondary pores on the pressure is illustrated in Fig. 7. It is shown that with increasing the pressure, the bulk density increases and the specific volume of secondary pores decreases. In

TABLE II The statistical data of pore distribution in MgO aggregates

Time (min)	Temperature (° C)						
	880					730	1030
	1.5	3.0	6.0	20	50	50	50
Specific volume of pore (ml g^{-1})	0.207	0.168	0.164	0.159	0.138	0.215	0.0803
Median (nm)	3.3	4.5	5.5	9.3	8.8	7.9	12.0
Mode (nm)	2.7	3.3	4.5	—	8.8	—	—
Shrinkage for magnesite (%)	28.68	34.37	34.95	35.66	38.75	27.43	47.25
Porosity of aggregates (%)	42.55	37.56	37.00	36.31	33.09	45.33	22.32

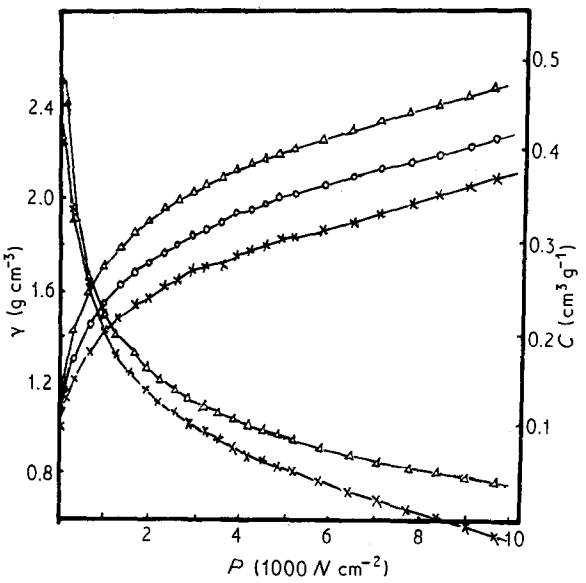

Figure 7 Dependence of bulk density and specific volume of secondary pores on pressure (△ calcined at 1030° C for 50 min, ○ 880° C for 50 min, × 730° C for 50 min).

addition, when the pressure is smaller than 10^{-3} N cm^{-2}, the specific volumes of secondary pores decrease rapidly with increasing pressure, but the differences between specific volumes of secondary pores of the samples calcined at 1030° C and that at 730° C are slight. It means that the pressure causes rearrangement of aggregates which results in a decrement of secondary pores. However, when pressure is more than 10^3 N cm^{-2}, the specific volume of the sample calcined at 730° C is smaller than that of samples calcined at 1030° C, which indicates that MgO powder obtained at 730° C has better compressibility, even though the bulk density of compacts made out of powder obtained at 1030° C is greater than obtained at 730° C. This implies that the MgO aggregates obtained at 730° C can be crushed more easily to fill the secondary pores, so that it is not reasonable to use green density as a parameter to evaluate the compressibility of the aggregated powder. The negatives at high pressure in Fig. 7 indicate that Equation 7 is not valid because a lot of aggregates are broken down.

Table III shows the pore distribution of compacts obtained by mercury porosimetry. The specific volumes of secondary pores (39.82–6237.0 nm) for the samples calcined at 730 and 880° C are almost the same, but the specific volume of secondary pores of sample calcined at 1030° C is larger; the reason is that the MgO aggregates formed at 1030° C are difficult to break down during compression.

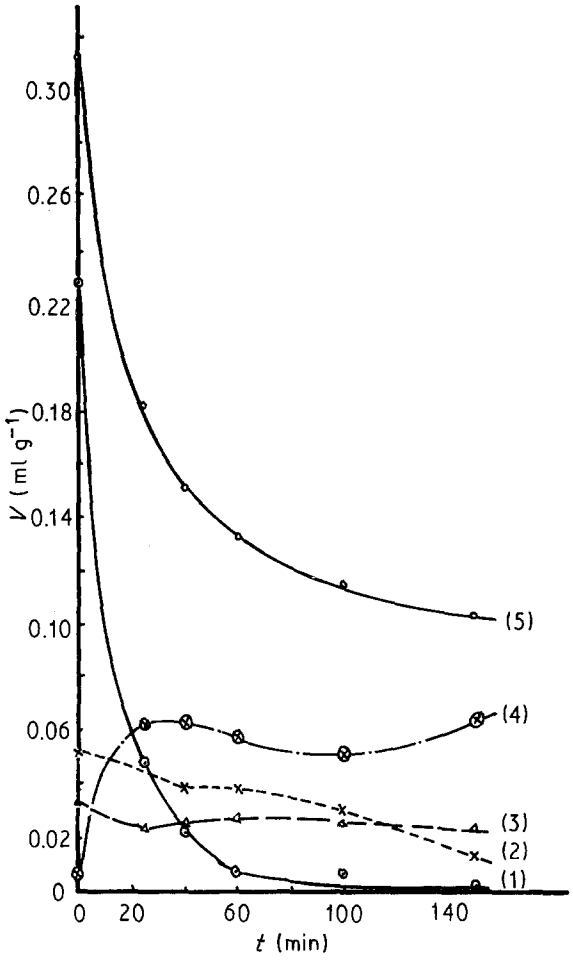

Figure 8 Dependences of specific volume of pores on sintering time (calcination temperature 730° C, sintering temperature 1180° C). (1) 2.19–39.82 nm, (2) 39.82–200.78 nm, (3) 200.78–396.78 nm, (4) 396.78–6237.0 nm, (5) 2.19–6237.0 nm.

4. Sintering of aggregated MgO compacts

The compacts were sintered at 1100, 1180, 1284 and 1397° C for the soaking times from 25 to 150 min. The pore distribution of compacts sintered was determined by mercury porosimetry. The results are shown in Figs 8 and 9. From Fig. 8, it can be seen that the specific volume of pores inside the aggregates reduces rapidly in the first 20 min, accompanied by an increase in the specific volume of the biggest pores (396.78–6237.0 nm), which means that the sintering of MgO crystallites within aggregates takes place rapidly. This sintering results in shrinkage of aggregates and causes rearrangement of aggregates and redistribution of pores. The rearrangement of aggregates and redistribution of pores were affected by the calcination temperature of magnesite. Fig. 9 compares the specific pore volume of compacts obtained at various calcination

TABLE III Distribution of pore volume of compacts (ml g^{-1})

Calcination temperature (° C)	Pore size (nm)			
	2.19–39.82	39.82–200.78	200.78–396.78	396.78–623.70
730	0.228 44	0.054 32	0.027 47	0.006 36
880	0.171 35	0.054 34	0.027 70	0.006 56
1030	0.094 71	0.052 01	0.030 08	0.023 70

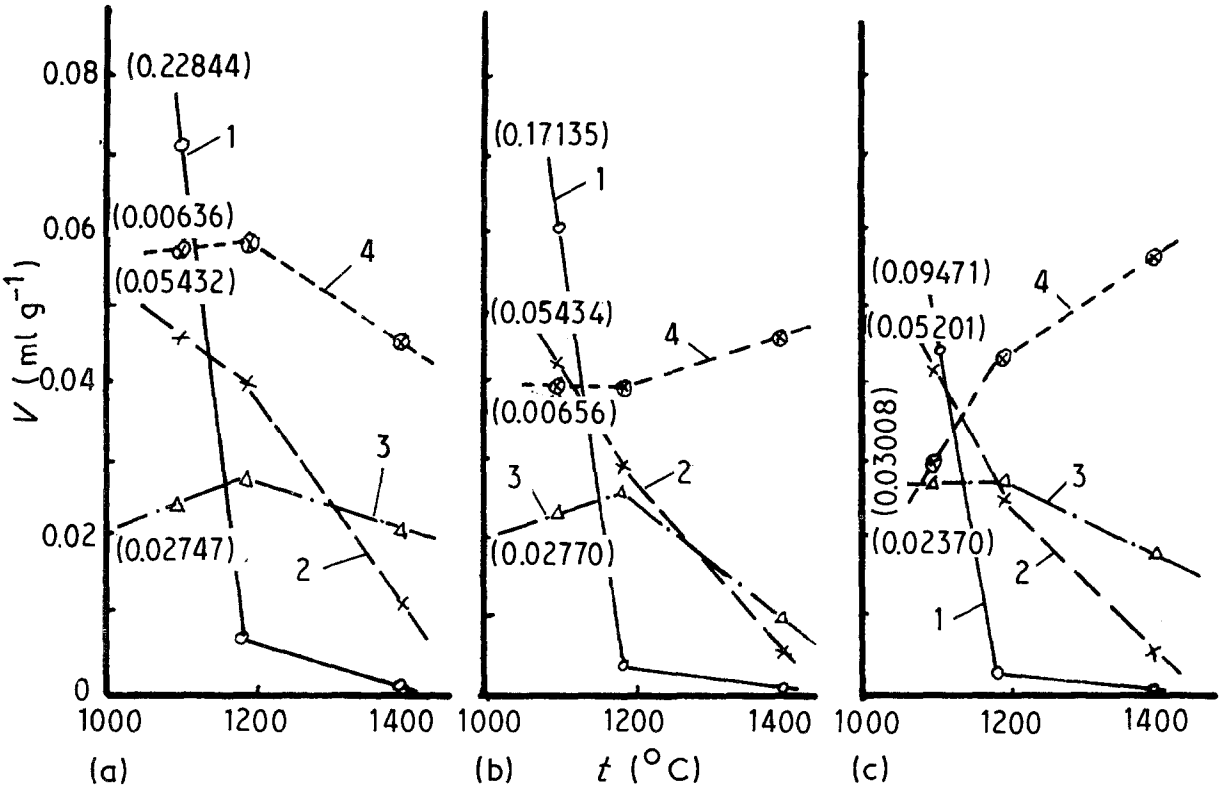

Figure 9 Dependence of specific volume of pores on sintering temperature ((a) calcined at 730° C, (b) at 880° C, (c) at 1030° C, sintering time 60 min. The figures in brackets at the starting end of lines are the specific values before sintering.)

temperatures. The aggregates were almost completely dense after sintering at 1200° C for 60 min. The samples obtained at various calcination temperatures display different features (Fig. 9). With increasing sintering temperature, the specific volume of big pores (396.78–6237.0 nm) of samples calcined at 730° C decreases, but that of samples calcined at 880 and 1030° C increases. The reason may be that the aggregates in the compacts made out of the powder calcined at 730° C were easily crushed during compaction to cause the changes of pore distribution and its coordination numbers which in turn influences sintering of aggregate compacts. Another reason may be that the differences of sinterability of MgO crystallites results in differences of shrinkage and rearrangement of aggregates.

Fig. 10 illustrates the total specific volume of pores of the samples made of the powders calcined at 730,

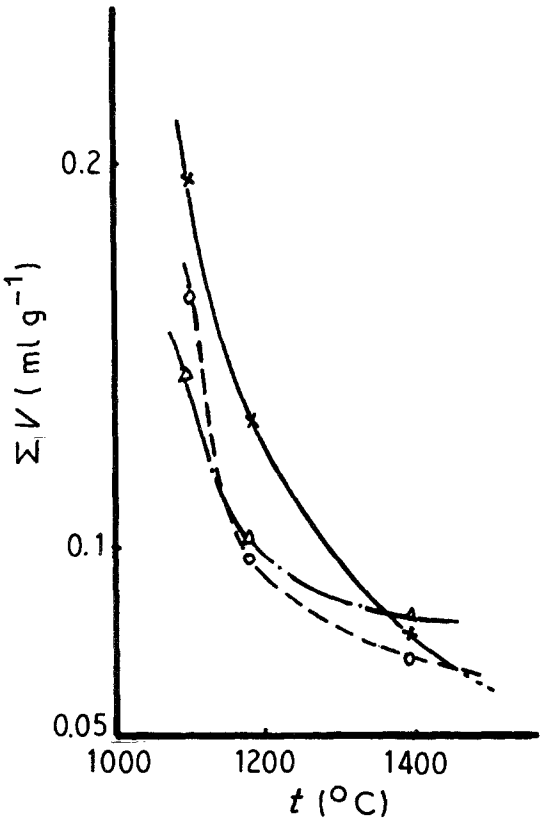

Figure 10 Total specific volume of pores as a function of sintered temperature (x 730° C (0.3166), o 880° C (0.2599), △ 1030° C (0.2005)) The figures in brackets are the values before sintering.

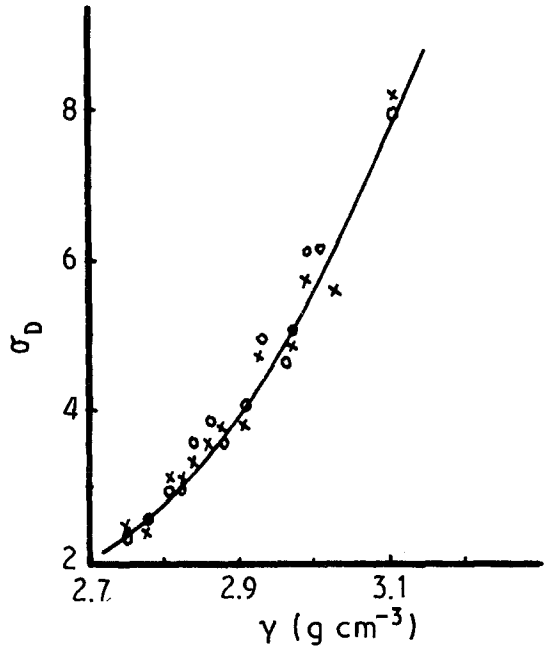

Figure 11 Standard deviation, σ_D plotted against bulk density, γ, of samples. (o planar, x spatial).

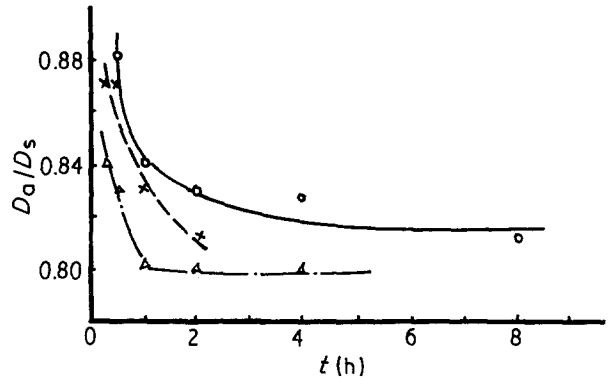

Figure 12 Shape parameter as a function of sintering time (○ 1500° C, × 1550° C, △ 1600° C).

880 and 1030° C as a function of sintering temperature. It can be expected that the end-point density of the sample made of the powder obtained at 730° C will be the largest among those of the three samples. The surface area of powder obtained at 730° C is equal to 58.30 $m^2 g^{-1}$, being very close to the optimum surface area value of about 60 $m^2 g^{-2}$, [10].

5. Grain size distribution and growth

To study the kinetics of grain growth, the compacts were preheated at 1200° C for 2 h and then isothermally sintered at 1500, 1550 and 1600° C for 0.25, 0.5, 1, 2, 4 and 8 h. The specimens were photomicrographed after they had been polished and HF etched. The two-dimensional diameter D_a and distribution were measured using a Magiscan-2 image analyser. The spatial diameter D_v and distribution were obtained by Schwartz–Saltikov transformation [11]. The number of grains measured were more than 1200.

It was found that the grain size parameters, both D_a and D_v, could be described by a log normal distribution. Equations 8 and 9 [12, 13] were used to calculate the parameters

$$D = \langle D \rangle = e^{\sigma^2/2} D_{med} \quad (8)$$

$$\sigma_D = D_{med}^2 e^{\sigma^2}(e^{\sigma^2} - 1) \quad (9)$$

where D is the mean diameter, D_{med} the mediam of the log normal distribution of D, and σ_D is the standard deviation of the normal distribution of ln D. Fig. 11 shows the relation between the standard deviation σ_D and bulk density. It indicates that with increasing density σ_D increases, which means that the distribution curve broadens.

The shape parameters D_a/D_s as a function of sintering time are shown in Fig. 12. Here D_a and D_s were calculated from the intersection area a and perimeter s, respectively.

$$D_a = (4a/\pi)^{1/2} \quad (10)$$

$$D_s = s/\pi \quad (11)$$

It can be seen that the shape parameters decrease rapidly in the first 1 or 2 h of sintering.

A parabolic growth law was confirmed for both two- and three-dimensional parameters

$$\text{For planar } \langle D \rangle^2 = Kt \quad (12)$$

$$\text{For spatial } D_{med}^2 = Gmt \quad (13)$$

The linear regression was used to fit the straight lines in Fig. 13, and the expressions are given as

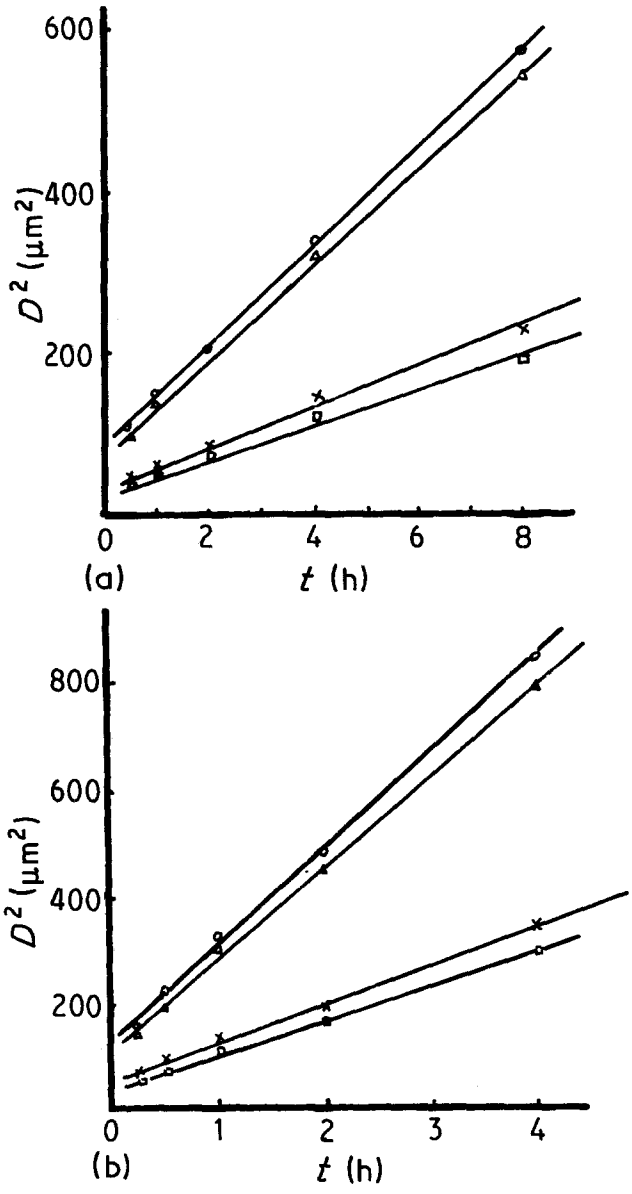

Figure 13 Plots of the square of grain size parameter, s, as a function of sintering time (○ $\langle D \rangle_3$, △ D_{med_3}, × $\langle D \rangle_2$, □ D_{med_2}) (a) 1500° C, (b) 1600° C and (c) 1550° C.

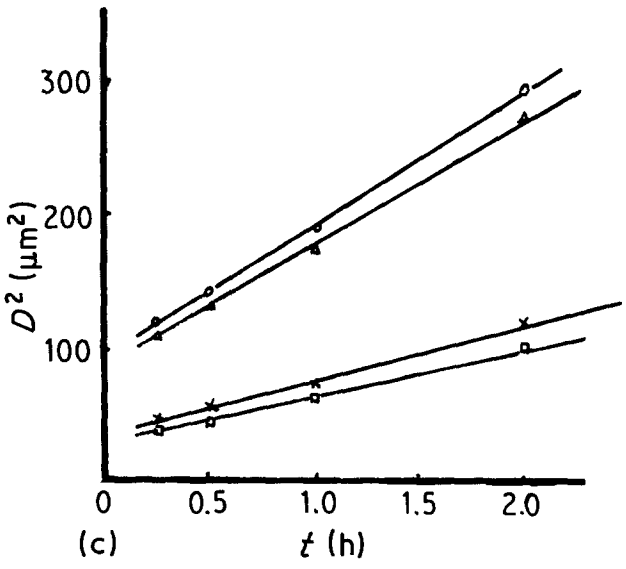

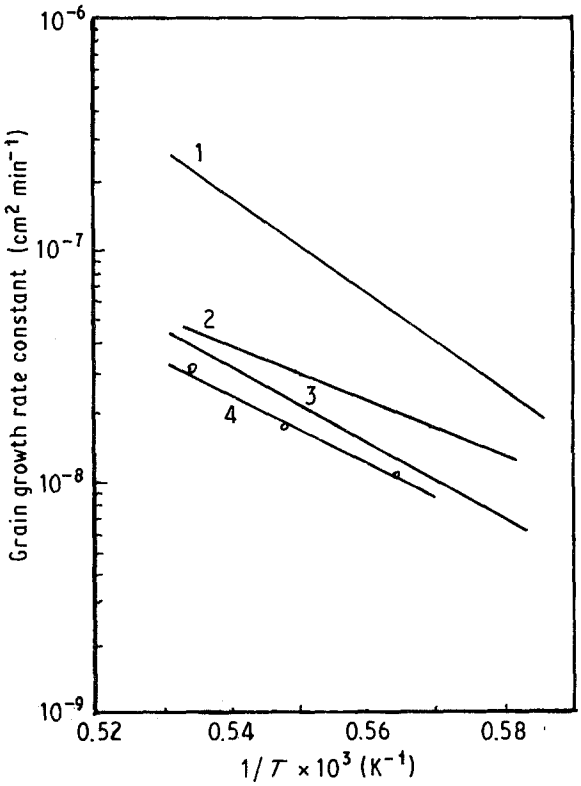

Figure 14 Arrhenius plot of the rate constant for $\langle D\rangle_3$. (1) Dense MgO, ΔH = 81 kcal mol^{-1} [14], (2) Porous MgO, ΔH = 60 kcal mol^{-1} [15], (3) Porous MgO, ΔH = 75.5 kcal mol^{-1} [16], (4) Porous MgO, ΔH = 70.9 kcal mol^{-1} (present study).

follows. For planar size parameters sintered at 1500° C,

$$D^2_{\text{med}_2} = 28.11 + 20.83t \quad (14)$$

$$\langle D\rangle^2_2 = 32.77 + 24.33t \quad (15)$$

sintered at 1550° C

$$D^2_{\text{med}_2} = 29.75 + 35.27t \quad (16)$$

$$\langle D\rangle^2_2 = 33.65 + 42.55t \quad (17)$$

sintered at 1600° C

$$D^2_{\text{med}_2} = 43.05 + 61.53t \quad (18)$$

$$\langle D\rangle^2_2 = 51.65 + 72.93t \quad (19)$$

For spatial size parameters sintered at 1500° C

$$D^2_{\text{med}_3} = 74.65 + 58.18t \quad (20)$$

$$\langle D\rangle^2_3 = 79.96 + 61.51t \quad (21)$$

sintered at 1550° C

$$D^2_{\text{med}_3} = 85.96 + 92.73t \quad (22)$$

$$\langle D\rangle^2_3 = 90.41 + 100.63t \quad (23)$$

sintered at 1600° C

$$D^2_{\text{med}_3} = 118.99 + 167.18t \quad (24)$$

$$\langle D\rangle^2_3 = 125.55 + 180.36t \quad (25)$$

The Arrhenius plot of the rate constant was shown in Fig. 14 compared with other authors' results [14–16].

From Fig. 14, the least squares gives

$$K = 9.24 \times 10^{-2} \exp\left(\frac{-70.9}{RT}\right)$$

$$(\text{kcal mol}^{-1}\,\text{cm}^2\,\text{sec}^{-1}) \quad (26)$$

and

$$Gm = 5.92 \times 10^{-2} \exp\left(\frac{-69.6}{RT}\right)$$

$$(\text{kcal mol}^{-1}\,\text{cm}^2\,\text{sec}^{-1}) \quad (27)$$

The activation energy obtained here is close to the values reported by Daniels (60 kcal mol^{-1}), Gupta (75.5 kcal mol^{-1}) and Kapadia (66 kcal mol^{-1}) [17]. However, it was found that K was two orders of magnitude smaller than the value reported by Kapadia [17] and one order larger than the value for MgO from alkoxide [18]. Besides the effect of composition, there may be another reason why the size distribution of particles and aggregates affect the size distribution and coordination number of pores which in turn influences the grain growth.

6. Summary

The sintering of MgO derived from natural magnesite was studied systematically. The important results are summarized as follows.

(1) The decomposition of magnesite takes place rapidly to form MgO crystallite aggregates which are sintered in further calcination. The sintering of MgO crystallites within aggregates can be divided into three stages: adjustment of structure, a process with few shrinkage of aggregates and a process with considerable shrinkage.

(2) It is not reasonable to use green density as a parameter to evaluate the compressibility of aggregate powder because the original difference of aggregate density causes error. The aggregated powder calcined at low temperature has good compressibility because the aggregates are easily broken down.

(3) MgO crystallites inside the aggregate have high sinterability. The pores in the aggregates almost disappear by sintering at temperatures as low as 1200° C. The rapid sintering of MgO crystallites inside the aggregates results in the shrinkage of aggregates and rearrangement of aggregates which causes the change of distribution of the pore size. This rearrangement depends upon the calcination condition and distribution of the size of the magnesite particles.

(4) The grain size distributions can be described by a log normal distribution. The grain growth obeys a parabolic law for both mean diameter and median diameter

$$\langle D\rangle^2 = Kt$$

$$D^2_{\text{med}} = Gt$$

Acknowlegement

This project was supported by the Science Fund of the Chinese Academy of Sciences.

References

1. CHENG RONGRONG and LI NAN, The Investigation on Kinetics of Sintering and Grain Growth of MgO during Calcination of Magnesite, 1987, accepted by J. Chinese Silicate Society.
2. LI NAN and CHENG RONGRONG, Compression and Sintering of MgO Derived from Magnesite, 1987, accepted by Refractories (China).
3. LI XIANG MING and LI NAN, The Investigation on

Kinetics of MgO Grain Growth, 1987, accepted by J. Wuhan, Iron and Steel University.
4. W. KOMATSU, Y. MORIYOSHI, S. K. MOON, H. KAMATA and S. KURASHIMA, *Yogyo-Kyokai-Shi* **10** (1977) 11.
5. R. M. GERMAN, *Sci. Sintering* **10** (1978) 11.
6. LI NAN and KE CHANGMING, *Sci. Sintering* **16** (1984) 91.
7. T. G. M. VAN DEN and R. J. HUNTER, *Rheologic Acta* **16** (1977) 534.
8. M. D. SACKS and J. A. PASK, *J. Amer. Ceram. Soc.* **65** (1982) 70.
9. F. F. LANGE, *ibid.* **67** (1984) 83.
10. LI NAN, CHEN SHIHUA and ZHAN DAOWENG, *Sci. Sintering* **19** (1987) 31.
11. E. E. UNDERWOOD, "Quantitative Stereology", (Addison-Wesley, Reading, Mass, 1970) Chaps 5 and 7.
12. S. K. KUTZ and F. M. A. CARPAY, *J. Appl. Phys.* **51** (1980) 5725.
13. *Idem., ibid.* **51** (1980) 5745.
14. R. M. SPRIGGS, L. A. BRISSETLE and T. VASILOS, *J. Amer. Ceram. Soc.* **47** (1964) 418.
15. A. U. DANIELS, R. C. LOWRIE, R. L. GIBBY and T. B. CUTLER, *J. Amer. Ceram. Soc.* **45** (1962) 282.
16. T. K. GUPTA, *J. Mater. Sci.* **6** (1971) 25.
17. C. M. KAPADIA and M. H. LEIPOLD, *J. Amer. Ceram. Soc.* **57** (1974) 41.
18. O. YAMAGUCHI, H. TONAMI, T. HAYASHI and K. SHIMIZU, *J. Jpn Soc. Powder Powder Metall.* **24** (1977) 157.

Received 12 October 1987
and accepted 28 April 1988